JSHC
Japan Society of
Histochemistry and Cytochemistry
Established 1959

Acta Histochem. Cytochem. 48 (1): 1–8, 2015
doi: 10.1267/ahc.14059

How Does the Ca^{2+}-paradox Injury Induce Contracture in the Heart? —A Combined Study of the Intracellular Ca^{2+} Dynamics and Cell Structures in Perfused Rat Hearts—

Hiroki Mani[1,2], Hideo Tanaka[1], Tetsuya Adachi[1], Masaya Ikegawa[3], Ping Dai[1], Naohisa Fujita[2] and Tetsuro Takamatsu[1]

[1]Department of Pathology and Cell Regulation, Kyoto Prefectural University of Medicine, Graduate School of Medical Science, [2]Department of Molecular Genetics and Laboratory Medicine, Kyoto Prefectural University of Medicine, Graduate School of Medical Science and [3]Department of Genomic Medical Sciences, Kyoto Prefectural University of Medicine, Graduate School of Medical Science, Kyoto 602–8566, Japan

Received November 21, 2014; accepted December 9, 2014; published online January 15, 2015

The calcium (Ca^{2+})-paradox injury of the heart, induced by restoration of extracellular Ca^{2+} after its short-term depletion, is known to provoke cardiomyocyte contracture. However, undetermined is how the Ca^{2+}-paradox provokes such a distinctive presentation of myocytes in the heart. To address this, we imaged sequential intracellular Ca^{2+} dynamics and concomitant structures of the subepicardial ventricular myocytes in fluo3-loaded, Langendorff-perfused rat hearts produced by the Ca^{2+} paradox. Under rapid-scanning confocal microscopy, repletion of Ca^{2+} following its depletion produced high-frequency Ca^{2+} waves in individual myocytes with asynchronous localized contractions, resulting in contracture within 10 min. Such alterations of myocytes were attenuated by 5-mM $NiCl_2$, but not by verapamil, SEA0400, or combination of ryanodine and thapsigargin, indicating a contribution of non-specific transmembrane Ca^{2+} influx in the injury. However, saponin-induced membrane permeabilization of Ca^{2+} showed no apparent contracture despite the emergence of high-frequency Ca^{2+} waves, indicating an essential role of myocyte-myocyte and myocyte-extracellular matrix (ECM) mechanical connections in the Ca^{2+} paradox. In immunohistochemistry Ca^{2+} depletion produced separation of the intercalated disc that expresses cadherin and dissipation of β-dystroglycan located along the sarcolemma. Taken together, along with the trans-sarcolemmal Ca^{2+} influx, disruption of cell-cell and cell-ECM connections is essential for contracture in the Ca^{2+}-paradox injury.

Key words: Ca^{2+} paradox, heart, Ca^{2+} wave, contracture, β-dystroglycan

I. Introduction

The Ca^{2+}-paradox injury, which is induced by short-term perfusion of the heart with Ca^{2+}-free solution (Ca^{2+} depletion) and subsequent reperfusion with Ca^{2+} (Ca^{2+} repletion), provokes irreversible intracellular Ca^{2+} ($[Ca^{2+}]_i$) overload and progressive contracture of cardiomyocytes [7, 25, 32, 33]. Because of the simple experimental procedure, the Ca^{2+} paradox is regarded as a useful experimental model for studying functional, morphological, and biochemical bases of myocardial injury, in particular $[Ca^{2+}]_i$ overload that simulates ischemia-reperfusion injury [25]. Despite such simple procedures, the mechanism(s) underlying the development of $[Ca^{2+}]_i$ overload is controversial [4, 7–9, 13, 15, 25]; some studies suggested that an influx of Ca^{2+} through either L-type Ca^{2+} channels [13, 15] or the Na^+-Ca^{2+} exchanger (NCX) in the cell membrane [8] is

Correspondence to: Hideo Tanaka, MD., PhD., Department of Pathology and Cell Regulation, Kyoto Prefectural University of Medicine, Graduate School of Medical Science, Kawaramachi Hirokoji, Kamigyo-Ku, Kyoto 602–8566, Japan. E-mail: hideotan@koto.kpu-m.ac.jp

responsible for the Ca^{2+} paradox-induced $[Ca^{2+}]_i$ overload, while others indicated the role of non-selective Ca^{2+} influx due to disruption of the cell membrane [4, 9]. In addition, electron microscopic studies suggested that the Ca^{2+} depletion-induced separation of the glycocalyx from the sarcolemma is speculated to be the cause of $[Ca^{2+}]_i$ overload [3, 10]. These different results stem from a lack of information regarding a direct link between structural changes and the concomitant $[Ca^{2+}]_i$ of the myocytes, in particular, exact sequential changes in myocyte morphology and $[Ca^{2+}]_i$ dynamics: morphological studies on the Ca^{2+}-paradox injury have hitherto been performed mostly on fixed preparations [4, 7–9, 13, 15, 25]. In addition to the mechanisms for $[Ca^{2+}]_i$ overload, it is also unsettled how the Ca^{2+}-paradox injury provokes myocyte contracture, the most distinctive presentation of the myocyte injury. In particular, unknown is whether the $[Ca^{2+}]_i$ overload is the only culprit for the contracture. With the advent of live-cell imaging technology, especially *in situ* real-time confocal microscopy, both the $[Ca^{2+}]_i$ dynamics and structure of the individual myocytes can be simultaneously visualized in the working heart [14, 18, 30]. This imaging modality, if applied to the heart under the Ca^{2+}-paradox injury, would enable us to address the mechanism(s) underlying development of myocyte contracture. The present study was undertaken to elucidate the mechanistic link between the development of $[Ca^{2+}]_i$ overload and the corresponding morphological changes in the Ca^{2+} paradox, and the related molecules responsible for the myocyte contracture in the heart.

II. Materials and Methods

Preparation of the heart for Ca^{2+} imaging

The investigation conformed with *the Guide for the Care and Use of Laboratory Animals* published by the US National Institutes of Health (NIH Publication No. 85-23, revised 1996) and was approved by the Institutional Committee for Animal Research (Approval reference No. M21-18). Adult male Wistar rats (9 weeks old) weighing 250–300 g were used (n=42). The procedure for *in situ* $[Ca^{2+}]_i$ imaging of the heart was essentially identical to those described previously [14, 18]. Briefly, Langendorff-perfused hearts with HEPES-buffered Tyrode's solution containing (in mM): NaCl 145, KCl 5.4, $MgCl_2$ 1, $CaCl_2$ 1, HEPES 10, and glucose 10 (pH=7.4 by NaOH) were loaded with fluo3/AM (22 μM; Dojin, Japan) at 19–21°C for 45 min. Following 15 min the hearts were perfused with Tyrode's solution containing probenecid (Nacalai Tesque, 1 mM) at 37°C for de-esterification of acetoxymethyl esters of fluo3/AM, and were subsequently used for experiments.

In situ real-time confocal microscopy

The confocal scanning system was principally analogous to that described by Hama *et al.* [14]. It consisted of a fixed stage upright microscope (BX50WI, Olympus), a multi-pinhole type confocal scanning device with a microlens array (CSU21, Yokogawa), an image intensifier (Videoscope, VS4-1845), an ICCD camera (310-TURBO, Roper), and a computer with an image capture board (IC-PCI, Imaging Technology). An Argon-Krypton laser beam focused with a water immersion objective lens (Olympus LUMPlan FL20X, numerical aperture=0.5) was applied to the subepicardial surface of the heart that was placed onto a custom-made perfusion chamber on the stage. The fluo3-fluorescence signals (8 bits, 512×480 pixels, 0.885 μm/pixel), scanned at 30 frames/sec on horizontal (X-Y) planes, were digitized with the ICCD camera, and were stored on a hard disc for later analysis.

Experimental procedures for the Ca^{2+} paradox

Before the Ca^{2+} paradox procedure the heart was perfused in a Langendorff manner at a constant rate of 10 mL/min with Ca^{2+}-containing (1 mM) Tyrode's solution under oxygenation with 100% O_2 at 25°C showing a regular sinus rhythm at 56±7 bpm (n=6). Stabilization of the heart with the Ca^{2+}-containing solution was followed by perfusion with Ca^{2+}-free Tyrode's for 10 min at 37°C (Ca^{2+} depletion) and for another 5 min at 25°C. Thereafter, the Ca^{2+} paradox was created by reperfusion with Ca^{2+}-containing (1 mM) solution (Ca^{2+} repletion). Upon repletion of Ca^{2+} the heart became pale due to the dissipation of the myoglobin (Fig. 1). Confocal visualization of $[Ca^{2+}]_i$ dynamics was made on the subepicardial myocardium at 25–26°C. In some hearts the cell membrane was stained with RH-237 (10 μM, Life Technologies) for visualization of the cell structure. Nickel chloride, verapamil, ryanodine, and thapsigargin were from Sigma, 2,3-butanedione monoxime (BDM), from Nacalai Tesque, and saponin, from Wako Pure Chemicals. SEA0400 was provided by Taisho Pharmaceutical Co., Ltd. [23].

Immunohistochemistry

The heart was fixed by perfusion with 2% paraformaldehyde for 30 min at room temperature for histochemical analysis. The fixed left ventricular free walls were cut into small pieces. Antibodies to β-dystroglycan (anti-mouse, monoclonal, Novo Castra) or to pan cadherin (anti-mouse, monoclonal, Abcam), diluted by 1:500, were applied to the specimen overnight at 4°C after 10-min treatment with 0.1% Triton X-100 and following 30-min treatment with 5% skim milk, and subsequently Alexa 488 goat anti-mouse IgG secondary antibody (Life Technologies) was applied for 2 hours at room temperature. Subepicardial myocytes of the left ventricle were imaged with a confocal laser scanning microscope (FV1000, Olympus) with a PlanApoN objective lens (60×, numerical aperture=1.42).

Two-dimensional blue native/SDS gel electrophoresis

Immunoblotting for β-dystroglycan was performed by a combination of blue native poly-acrylamide gel electrophoresis (BN-PAGE) and sodium dodecyl sulfate

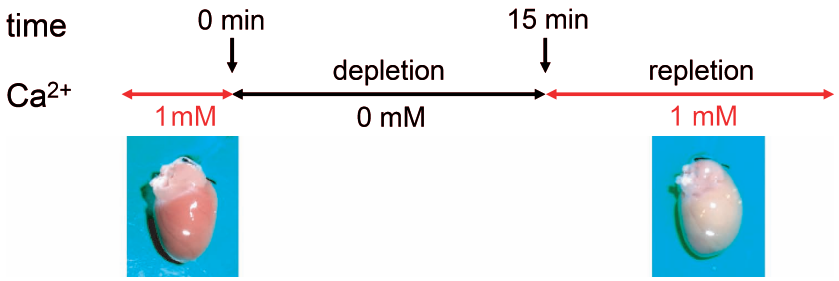

Fig. 1. Schematic representation of procedure for Ca^{2+}-paradox experiment and gross images of the heart before Ca^{2+} depletion (left) and after Ca^{2+} repletion (right).

poly-acrylamide gel electrophoresis (SDS-PAGE) in a two-dimensional approach [5]. The excised rat heart, after washout of the blood with Tyrode's solution, was subjected to the analysis. The whole cell lysates after SDS-PAGE, separated of protein complex via BN-PAGE, were compared before and during Ca^{2+} depletion.

Data analysis

Analysis of the *in situ* confocal real-time image was conducted on the digitized fluorescence intensity for fluo3 and RH-237 by Image J software (NIH). Quantitative analyses of Ca^{2+} waves were performed from X-t images, which were reconstructed by cumulatively layering a series of consecutive X-Y image frames scanned by a line along the longitudinal axis of the cells. The cell length and intercellular gap were measured from X-Y images stained with RH-237. In immunohistochemistry, intensity of the Alexa 488 fluorescence was analyzed by averaging the fluorescence intensity along the cell membrane at 10-μm length. The quantitative data (mean±SD) were statistically analyzed by ANOVA, and significance was defined as $P<0.05$.

III. Results

Changes in $[Ca^{2+}]_i$ dynamics and cell structure by Ca^{2+} paradox

The $[Ca^{2+}]_i$ dynamics of cardiomyocytes were distinct among the three different conditions; i.e., before and during Ca^{2+} depletion, and after Ca^{2+} repletion (Figs. 2 and 3). Under control conditions (Fig. 2A) the myocytes exhibited spatially homogenous Ca^{2+} transients on excitation with no discernible rise of $[Ca^{2+}]_i$ during diastole as shown in the sequential X-Y (Fig. 2A-b) and X-t (cells 1–3 in Fig. 2A-c) images. The corresponding fluorescent image of the cell membranes stained with RH-237 indicated that the individual myocytes showed tight connections at the intercalated discs (Fig. 2A-a). In sharp contrast, depletion of extracellular Ca^{2+} diminished Ca^{2+} transients, and instead, Ca^{2+} waves emerged sporadically in individual cells (Fig. 2B). The waves occurred within the myocytes (Fig. 2B-a) at an incidence of 11.7±3.8/min/cell showing longitudinal propagation at a velocity (V_{prop}) of 77.5±13.5 μm/sec (n=33). Of note, myocytes appeared disconnected at intercalated discs having a remarkable intercellular gap (approx. 7 μm) during Ca^{2+} depletion (Fig. 2B-b). Upon repletion of Ca^{2+} high-frequency, ripple-like Ca^{2+} waves developed in individual myocytes (Fig. 3) within 2 min. Such high-frequency Ca^{2+} waves were asynchronous among the myocytes at a frequency of 123.3±21.0/min/cell with V_{prop} of 90.4±21.1 μm/sec (n=23), and were accompanied by localized, wave-like contractions as evident in fluctuations of the intercellular gaps (Fig. 3b). Moreover, intercellular gaps widened gradually and myocytes eventually showed contracture (Fig. 3c) after 10-min of Ca^{2+} repletion, where myocytes exhibited no apparent Ca^{2+} waves, but instead showed high-static fluo3-fluorescence intensity.

Role of transmembrane Ca^{2+} influx in the Ca^{2+} paradox-induced contracture

Sequential changes in the intercellular gap and myocyte length revealed that the gap gradually widened with concomitant shortening of the cells having a sigmoid time course of changes in cell length with a half shortening time of 3.3±0.6 min (Fig. 4). We also examined the time courses of changes in the myocyte length and intercellular gap under pharmacological inhibition of various pathways for the $[Ca^{2+}]_i$ rise. In the presence of SEA0400 (3 μM), a selective inhibitor of the NCX, the Ca^{2+} paradox-induced emergence of Ca^{2+} waves and contracture were not attenuated: the time course of changes in cell length and the properties of Ca^{2+} waves were identical to those found in the absence of this agent (Fig. 5). Blockade of L-type Ca^{2+} channels by verapamil (20 μM) also resulted in progressive contracture with concomitant Ca^{2+} waves with the incidence and V_{prop} equivalent to those in the absence of the drug, although the latent period for cell shortening was prolonged for about 2.5 min (Fig. 5). Diminution of Ca^{2+} release from the sarcoplasmic reticulum (SR) by combined application of ryanodine (10 μM) and thapsigargin (0.5 μM) also failed to prevent the contracture: time courses of the changes in cell length were almost identical to those in the absence of these inhibitors (Fig. 5A). In contrast, nickel chloride (5 mM) was effective in preventing the progressive contracture and $[Ca^{2+}]_i$ overload, where myocytes exhibited neither Ca^{2+} waves, wave-like contractions, nor widening of the intercalated discs (Fig. 5).

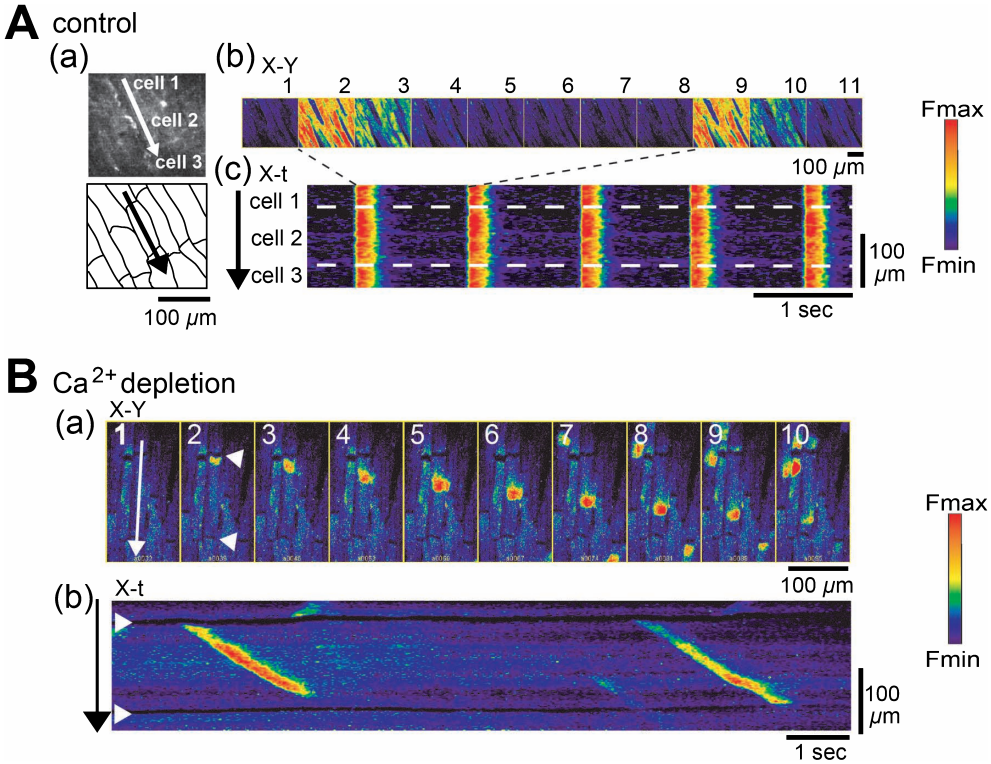

Fig. 2. The $[Ca^{2+}]_i$ dynamics of the subepicardial surface of the left ventricle in the Langendorff-perfused rat heart before (**A**) and during (**B**) Ca^{2+} depletion. **A(a)**: An X-Y image stained with RH-237 and the corresponding schematic illustration of myocytes at the same region. **A(b)**: Sequential X-Y images (1–11, displayed every 150 msec) of the $[Ca^{2+}]_i$ dynamics before Ca^{2+} depletion. The individual myocytes show homogenous Ca^{2+} transients (2 and 9) on excitation. **A(c)**: An X-t image of the myocytes (cells 1–3) scanned along the arrow in **A(a)**. The dotted lines denote the cell borders. **B**: The $[Ca^{2+}]_i$ dynamics during Ca^{2+} depletion. **B(a)**: Sequential X-Y images (1–10) displayed every 210 msec. **B(b)**: X-t image of the cells indicated by an arrow in **B(a)**. The myocytes exhibit Ca^{2+} waves propagating sporadically along the longitudinal axis instead of Ca^{2+} transients. Note that the cells are separated at intercalated discs (indicated by two white arrowheads).

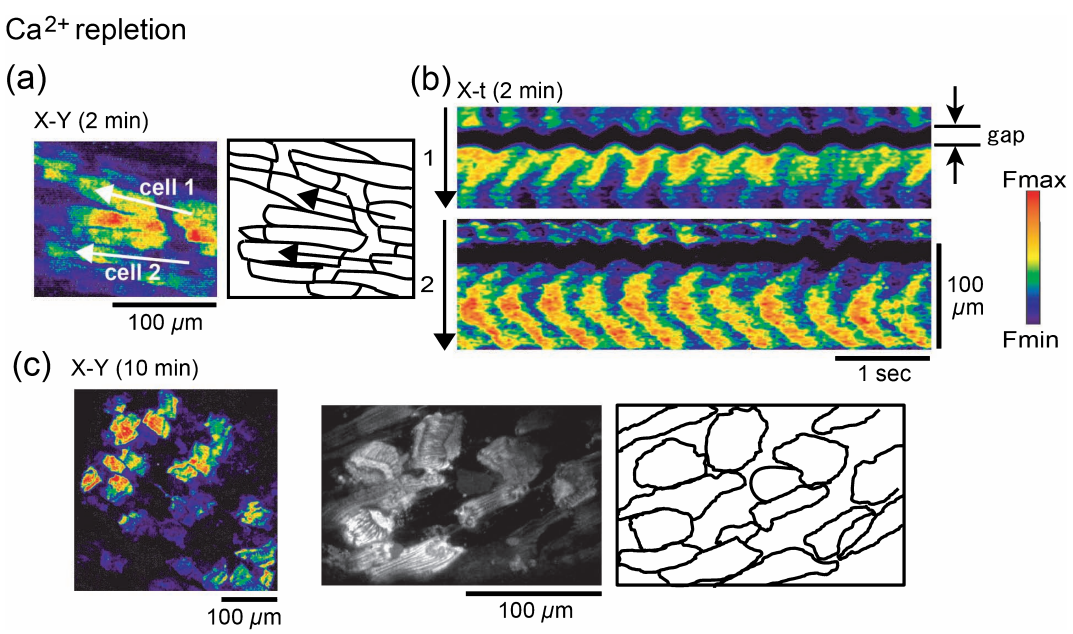

Fig. 3. The $[Ca^{2+}]_i$ dynamics of the subepicardial surface of the left ventricle in the Langendorff-perfused rat heart after Ca^{2+} repletion. **(a)**: The X-Y fluo3-fluorescence image recorded 2 min after Ca^{2+} repletion and the corresponding outline drawing are shown on the right panel. **(b)**: Two X-t images of myocytes showing high-frequency Ca^{2+} waves with asynchronous localized contractions are shown. Note that the intercalated disc is remarkably detached (indicated by "gap"). **(c)**: Shown are X-Y images (left, fluo3 fluorescence; middle, RH-237) of the myocytes acquired 10 min after Ca^{2+} repletion and the corresponding outline drawing on the right panel. Cells are remarkably detached from the intercalated discs showing contracture.

Role of $[Ca^{2+}]_i$ overload and mechanical motion in the development of contracture

When myocytes were rendered $[Ca^{2+}]_i$ overload by membrane permeabilization with saponin (0.4%, 0.1 mM-Ca^{2+}-containing Tyrode's solution), they showed high-frequency Ca^{2+} waves (Fig. 6A) at 120.8±8.5/min/cell showing rapid V_{prop} of 117.7±11.0 μm/sec (n=33, 3 hearts) and asynchronous wave-like contractions; the former values were similar to, and the latter, significantly higher than, those observed in Ca^{2+}-paradox injury (Fig. 6B-a, b). However, the saponin treatment failed to mimic the Ca^{2+}-paradox injury; no widening of the intercellular gap or myocyte contracture occurred (Fig. 6B-c). Thus, irreversible $[Ca^{2+}]_i$ overload by trans-membrane Ca^{2+} influx alone did not lead to development of the contracture.

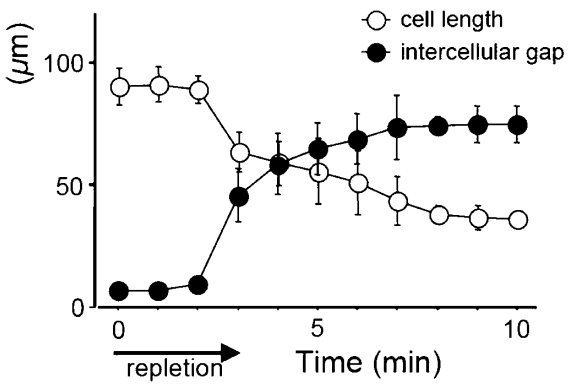

Fig. 4. Sequential changes in cell length and intercellular gap during Ca^{2+} repletion. Time zero denotes the start of Ca^{2+} repletion.

In the presence of the mechanical uncoupler BDM [21] at 30 mM, no myocyte contracture occurred after Ca^{2+} repletion, where most myocytes exhibited quiescent $[Ca^{2+}]_i$ without contraction, and Ca^{2+} waves or excitation-evoked Ca^{2+} transients were barely observed. However, washing out of BDM during Ca^{2+} repletion resulted in emergence of high-frequency Ca^{2+} waves with asynchronous local contractions of individual myocytes and eventual contracture (3 hearts, data not shown). Thus, mechanical contraction *per se* is indispensable for contracture.

Immunohistochemistry for cadherin and β-dystroglycan

Contraction of the myocytes is mediated by the costameres, which physically connect the myofilaments to the extracellular matrix (ECM) via dystroglycan complex [6, 16, 20]. To test whether or not Ca^{2+} depletion alters β-dystroglycan, we conducted immunohistochemistry for this protein. In intact hearts β-dystroglycan was expressed continuously along the cell membranes, whereas depletion of Ca^{2+} remarkably reduced the distribution of this protein (Fig. 7A-a). Quantitatively the fluorescence intensity for β-dystroglycan was significantly reduced by Ca^{2+} depletion (Fig. 7A-b). Furthermore, two-dimensional gel immunoblotting for β-dystroglycan revealed that multiple protein complexes were identified during control, whereas the largest component of the complex was significantly diminished by Ca^{2+} depletion (Fig. 7A-c). In addition, immunohistochemistry revealed that separation of intercalated discs produced by Ca^{2+} depletion was associated with detachment of cadherin (Fig. 7B). Thus, Ca^{2+} depletion appeared to dimin-

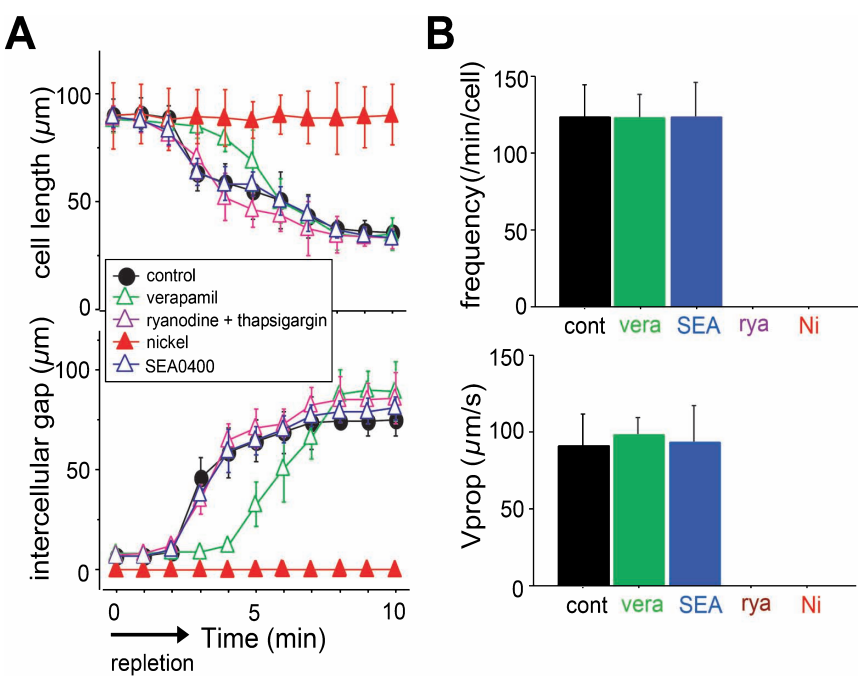

Fig. 5. **A**: Pharmacological effects on the sequential changes in cell length (upper) and intercellular gap (lower) during Ca^{2+} repletion. **B**: The bar graphs showing frequency (upper) and propagation velocity, V_{prop}, (lower) of Ca^{2+} waves during Ca^{2+} repletion under various pharmacological interventions. The acronym 'cont' denotes control, "vera", verapamil at 20 μM, "SEA", SEA0400 at 3 μM, "rya", ryanodine at 10 μM and thapsigargin at 0.5 μM, and "Ni", nickel chloride at 5 mM.

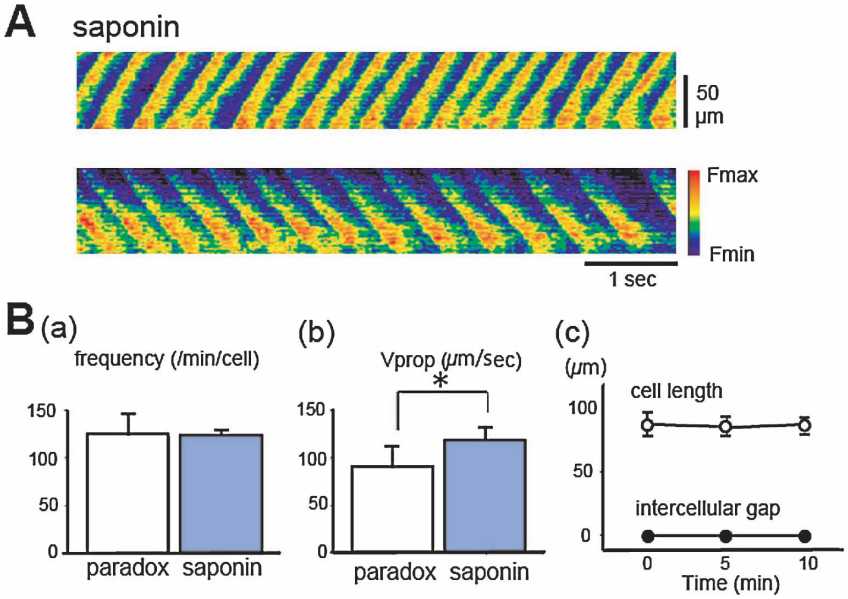

Fig. 6. Effects of membrane permeabilization on Ca^{2+} waves and myocyte shortening. **A**: Two representative X-t images of $[Ca^{2+}]_i$ dynamics after application of saponin. Saponin (0.4% in 0.1 mM Ca^{2+}-containing Tyrode's solution) produced high-frequency, rapidly propagating Ca^{2+} waves in individual myocytes. **B**: Frequency **(a)** and V_{prop} **(b)** of Ca^{2+} waves during saponin perfusion compared with those induced by Ca^{2+} paradox. **(c)** Time course of the myocyte dimensions, cell length and intercellular gap, before and during perfusion with saponin at 5 and 10 min. *, P<0.01.

ish β-dystroglycan along the sarcolemmal membrane, in addition to the separation of cadherin at the intercalated disc.

IV. Discussion

The present study addressed the mechanisms for myocyte contracture produced by Ca^{2+}-paradox injury in the heart. On restoration of extracellular Ca^{2+} following short-term Ca^{2+} depletion in the Langendorff-perfused rat heart, individual cardiomyocytes exhibited asynchronous, high-frequency Ca^{2+} waves. Ca^{2+} waves of this type would correspond to the "agonal" waves we previously identified in the rat heart [18, 30], a presentation of irreversible $[Ca^{2+}]_i$ overload leading to cell death. Such irreversible $[Ca^{2+}]_i$ dynamics accompanied the progressive contracture of the myocytes with a sigmoid time course of the cell-length shortening during the Ca^{2+} repletion. This sequence of events was nearly superimposable on that under blockade of either NCX or SR Ca^{2+} release, indicating no major role of these Ca^{2+} handling proteins in the contracture. A slight retardation of the development of contracture by verapamil (~2.5 min) may indicate a minor, if any, contribution of the voltage-gated L-type Ca^{2+} channels to this phenomenon. The Ca^{2+} paradox-induced contracture was found to be mediated by transmembrane influx of Ca^{2+} via Ni^{2+}-sensitive pathway(s) other than the L-type Ca^{2+} channels or NCX, e.g., Ca^{2+}-permeable non-specific cation channels [24], although no definitive pathway was eventually specified in this study. A relatively recent study in isolated mouse ventricular myocytes suggested that transient receptor potential (TRP) channels mediate the influx of Ca^{2+} under the Ca^{2+}-paradox injury [19]. Considering that the TRP channels are activated by various environmental changes, in particular, mechanical stretch [22], the myocyte contraction *per se* may contribute to the development of $[Ca^{2+}]_i$ overload via this channel. In practice, we observed that mechanical arrest by BDM precluded the generation of the high-frequency Ca^{2+} waves, whereas its washout resulted in generation of the agonal waves and hypercontracture. This indicates that certain mechano-sensitive pathway(s) may provide progressive, synergistic augmentation of $[Ca^{2+}]_i$ overload through the transmembrane influx of Ca^{2+}. It remains to be determined whether or not the TRP channels are the culprit for the irreversible $[Ca^{2+}]_i$ overload in the multicellular myocardium.

The key finding of this study is that the massive trans-sarcolemmal influx of Ca^{2+}, presented as the high-frequency Ca^{2+} waves, was not sufficient for the development of contracture, because saponin-induced Ca^{2+} permeabilization of the membrane barely produced myocyte separation or contracture despite the severe $[Ca^{2+}]_i$ overload that was equivalent to that emerged during the Ca^{2+}-paradox injury. Two major alterations were identified under Ca^{2+} depletion: separation of the myocytes at intercalated discs and dissipation of the β-dystroglycan complex along the lateral membrane surface of the myocytes. The former change would stem from impairment of the Ca^{2+}-dependent intercellular connection at the intercalated disc via N-cadherin [17] as confirmed by its separation in immunohistochemistry. Such cell-end to cell-end separation of the myocytes, however, would not fulfill the requirement for the hypercontracture, because myocytes are tightly connected to the lateral sides with the ECM, i.e., the scaffold

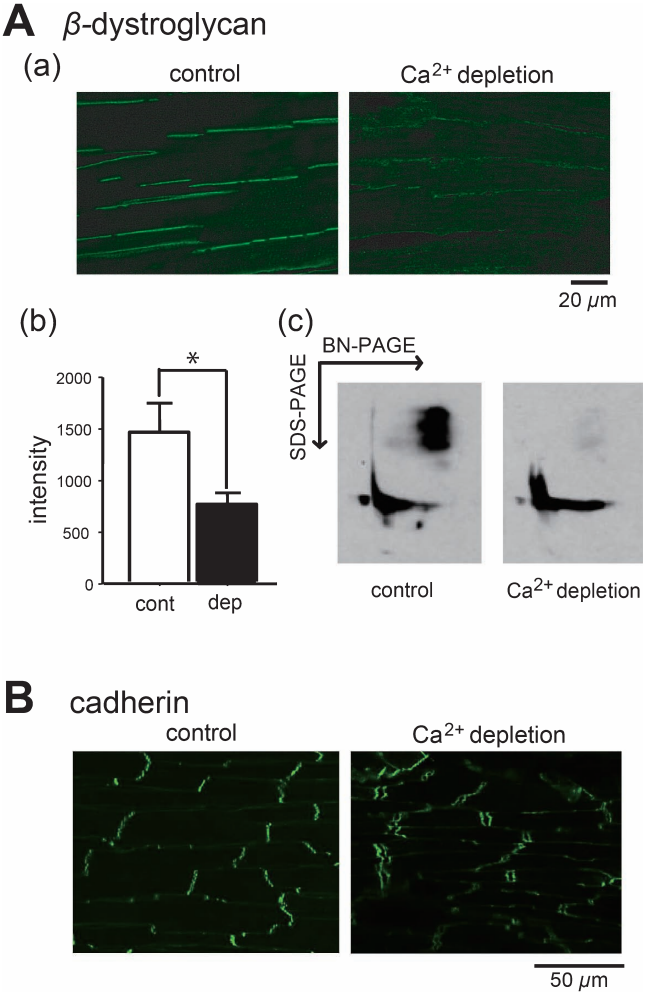

Fig. 7. **A**: **(a)** Immunohistochemical images of β-dystroglycan before (control) and during Ca^{2+} depletion. β-dystroglycan was distributed continuously along cell membranes, whereas its distribution was reduced after 10-min depletion of Ca^{2+}. **(b)**: Comparison of fluorescence intensity for β-dystroglycan under control conditions (cont) and during Ca^{2+} depletion (dep). *, $P<0.01$. **(c)**: Two-dimensional blue native/SDS gel electrophoresis for β-dystroglycan before and during Ca^{2+} depletion. **B**: Immunohistochemistry of cadherin of the heart before and during Ca^{2+} depletion.

of the myocardium [6, 16, 20]. We assume the deletion of β-dystroglycan by Ca^{2+} depletion is responsible for the progressive contracture in the Ca^{2+}-paradox injury because this membrane-spanning protein forms a complex that connects with the actin-binding protein dystrophin in the cells [6, 16, 20, 26], and provides trans-sarcolemmal linkage between the actin filaments and the ECM at the costamere. Thus, in addition to the separation of the cell-cell connection via N-cadherin, weakening of the cell-ECM connection by diminution of β-dystroglycan, may lead to the contracture. Although it may be practically difficult to address the role of β-dystroglycan in the development of contracture, an instantaneous, whole-cell ablation of this target protein, by using chromophore-assisted laser inactivation (CALI) [28, 29], may provide a direct evidence for this assumption.

At present it is unknown how Ca^{2+} depletion leads to dissipation of β-dystroglycan. In this regard, Rentschler *et al.* [26] identified Ca^{2+}-binding EF-hand regions in dystrophin that are essential for binding with β-dystroglycan. This may indicate that Ca^{2+} depletion promotes detachment of β-dystroglycan from dystrophin by impairment of these regulatory sites, and thereby, diminishes β-dystroglycan located along the cell membrane. It is also undetermined whether and how the depletion of β-dystroglycan contributes to irreversible Ca^{2+} influx in the myocytes. In this respect, dissipation of the dystroglycan-dystrophin complex in the skeletal muscle of the muscular dystrophy (mdx) mice reportedly promotes Ca^{2+} influx via Ca^{2+} leakage [1, 2] due possibly to disruption of the membrane integrity and subsequent activation of protease(s), e.g., calpain, and thereby, augment permeability of the cell membrane to Ca^{2+}. In practice, mediation of calpain was suggested in the Ca^{2+}-paradox injury of the heart [11, 31]. It should also be noteworthy that mdx skeletal muscles showed increased expression of TRP channels [12].

To our knowledge the present observations are the first to propose a possible contribution of cell-ECM disconnection by dissipation of β-dystroglycan and the resultant $[Ca^{2+}]_i$ overload in the development of myocyte contracture under the Ca^{2+}-paradox injury. Our experimental design, however, may not directly reflect the real pathological conditions in the heart. In this regard, as Rodriguez *et al.* [27] demonstrated, several membrane-spanning proteins including β-dystroglycan are predominantly diminished in ischemic myocardium. Thus, during ischemia-reperfusion injury, alterations of β-dystroglycan may contribute to impairment of the structure and mechanical functions of the myocardium. Our present results provide important insights into the mechanism for myocardial injury that leads to contracture.

V. Disclosures

None.

VI. Acknowledgment

This work was supported by a Grant-in-Aid for Scientific Research from the Ministry of Education, Culture, Sports, Science and Technology of Japan.

VII. References

1. Alderton, J. M. and Steinhardt, R. A. (2000) How calcium influx through calcium leak channels is responsible for the elevated levels of calcium-dependent proteolysis in dystrophic myotubes. *Trends Cardiovasc. Med.* 10; 268–272.
2. Alderton, J. M. and Steinhardt, R. A. (2000) Calcium influx through calcium leak channels is responsible for the elevated levels of calcium-dependent proteolysis in dystrophic myotubes. *J. Biol. Chem.* 275; 9452–9460
3. Ashraf, M. (1979) Correlative studies on sarcolemmal ultrastructure, permeability, and loss of intracellular enzymes in

the isolated heart perfused with calcium-free medium. *Am. J. Pathol.* 97; 411–432.
4. Bosteels, S., Matejovic, P., Flameng, W. and Mubagwa, K. (1999) Sodium influx via a non-selective pathway activated by the removal of extracellular divalent cations: possible role in the calcium paradox. *Cardiovasc. Res.* 43; 417–425.
5. Camacho-Carvajal, M. M., Wollscheid, B., Aebersold, R., Steinmle, V. and Schamel, W. A. (2004) Two-dimensional blue native/SDS gel electrophoresis of multi-protein complexes from whole cellular lysates. *Mol. Cell. Proteomics* 3; 176–182.
6. Campbell, K. P. (1995) Three muscular dystrophies: loss of cytoskeleton-extracellular matrix linkage. *Cell* 80; 675–679.
7. Chapman, R. A. and Tunstall, J. (1987) The calcium paradox of the heart. *Prog. Biophys. Mol. Biol.* 50; 67–96.
8. Chatamra, K. R. and Chapman, R. A. (1996) The effects of sodium-calcium exchange inhibitors on protein loss associated with the calcium paradox of the isolated Langendorff perfused guinea-pig heart. *Exp. Physiol.* 81; 203–210.
9. Diederichs, F. (1994) Intracellular free Ca^{2+}, Na^{+}, and H^{+} concentrations in the isolated perfused rat heart during the Ca^{2+} paradox. *Cell Calcium* 15; 297–304.
10. Frank, J. S., Langer, G. A., Nudd, L. M. and Seraydarian, K. (1977) The myocardial cell surface, its histochemistry, and the effect of sialic acid and calcium removal on its structure and cellular ionic exchange. *Circ. Res.* 41; 702–714.
11. Gaitanaki, C., Papazafiri, P. and Beis, I. (2003) The calpain-caplastatin system and the calcium paradox in the isolated perfused pigeon heart. *Cell. Physiol. Biochem.* 13; 173–180.
12. Gervásio, O. L., Whitehead, N. P., Yeung, E. W., Phillips, W. D. and Allen, D. G. (2008) TRPC1 binds to caveolin-3 and is regulated by Src kinase—role in Duchenne muscular dystrophy. *J. Cell Sci.* 121; 2246–2255.
13. Grinwald, P. M. and Nayler, W. G. (1981) Calcium entry in the calcium paradox. *J. Mol. Cell. Cardiol.* 13; 867–880.
14. Hama, T., Takahashi, A., Ichihara, A. and Takamatsu, T. (1998) Real time in situ confocal imaging of calcium wave in the perfused whole heart of the rat. *Cell. Signal.* 10; 331–337.
15. Hearse, D. J., Baker, J. E. and Humphrey, S. M. (1980) Verapamil and the calcium paradox. *J. Mol. Cell. Cardiol.* 12; 733–739.
16. Henry, M. D. and Campbell, K. P. (1999) Dystroglycan inside and out. *Curr. Opin. Cell Biol.* 11; 602–607.
17. Hertig, C. M., Butz, S., Koch, S., Eppenberger-Eberhardt, M., Kemler, R. and Eppenberger, H. M. (1996) N-cadherin in adult rat cardiomyocytes in culture. *J. Cell Sci.* 109; 11–20.
18. Kaneko, T., Tanaka, H., Oyamada, M., Kawata, S. and Takamatsu, T. (2000) Three distinct types of Ca^{2+} waves in Langendorff-perfused rat heart revealed by real-time confocal microscopy. *Circ. Res.* 86; 1093–1099.
19. Kojima, A., Kitagawa, H., Omatsu-Kanbe, M., Matsuura, H. and Nosaka, S. (2010) Ca^{2+} paradox injury mediated through TRPC channels in mouse ventricular myocytes. *Br. J. Pharmacol.* 161; 1734–1750.
20. Lapidos, K. A., Kakkar, R. and McNally, E. M. (2004) The dystrophin glycoprotein complex: signaling strength and integrity for the sarcolemma. *Circ. Res.* 94; 1023–1031.
21. Li, T., Sperelakis, N., TenEick, R. E. and Solaro, R. J. (1985) Effects of diacetyl monoxime on cardiac excitation-contraction coupling. *J. Pharmacol. Exp. Ther.* 232; 688–695.
22. Maroto, R., Raso, A., Wood, T. G., Kurosky, A., Martinac, B. and Hamill, O. P. (2005) TRPC1 forms the stretch-activated cation channel in vertebrate cells. *Nat. Cell Biol.* 7; 179–185.
23. Matsuda, T., Arakawa, N., Tamura, K., Kishida, Y., Kawasaki, Y., Sakaue, M., Takahashi, K., Takahashi, T., Suzuki, T., Ota, T., Hamano-Takahashi, A., Onishi, M., Tanaka, Y., Kameo, K. and Baba, A. (2001) SEA0400, a novel and selective inhibitor of the Na^{+}-Ca^{2+} exchanger, attenuates reperfusion injury in the in vitro and in vivo cerebral ischemic models. *J. Pharmacol. Exp. Ther.* 298; 249–256.
24. McCarter, G. C. and Steinhardt, R. A. (2000) Increased activity of calcium leak channels caused by proteolysis near sarcolemmal ruptures. *J. Membr. Biol.* 176; 169–174.
25. Piper, H. M. (2000) The calcium paradox revisited: an artefact of great heuristic value. *Cardiovasc. Res.* 45; 123–127.
26. Rentschler, S., Linn, H., Deininger, K., Bedford, M. T., Espanel, X. and Sudol, M. (1999) The WW domain of dystrophin requires EF-hands region to interact with β-dystroglycan. *Biol. Chem.* 380; 431–442.
27. Rodriguez, M., Cai, W.-J., Kostin, S., Lucchesi, B. R. and Schaper, J. (2005) Ischemia depletes dystrophin and inhibits protein synthesis in the canine heart: mechanisms of myocardial ischemic injury. *J. Mol. Cell. Cardiol.* 38; 723–733.
28. Sano, Y., Watanabe, W. and Matsunaga S. (2014) Chromophore-assisted laser inactivation—towards a spatiotemporal-functional analysis of proteins, and the ablation of chromatin, organelle and cell function. *J. Cell Sci.* 127; 1621–1629.
29. Tanabe, T., Oyamada, M., Fujita, K., Dai, P., Tanaka, H. and Takamatsu, T. (2005) Multiphoton excitation-evoked chromophore-assisted laser inactivation using green fluorescent protein. *Nat. Methods* 2; 503–505.
30. Tanaka, H. and Takamatsu, T. (2003) Spatiotemporal visualization of intracellular Ca^{2+} in living heart muscle cells viewed by confocal laser scanning microscopy. *Acta Histochem. Cytochem.* 36; 193–204.
31. Zhang, J.-Y., Tong, W., Wu, F., Bi, S.-H., Xu, M., Jin, Z.-X., Yang, Y., Jaing, X.-F. and Zhou, J.-J. (2012) Different roles for contracture and calpain in calcium paradox-induced heart injury. *PLoS ONE* 7; e52270.
32. Zimmerman, A. N. E. and Hulsmann, W. C. (1966) Paradoxical influence of calcium ions on the permeability of the cell membranes of the isolated rat heart. *Nature* 211; 646–647.
33. Zimmerman, A. N. E., Daems, W., Hulsmann, W. C., Snijder, J., Wisse, E. and Durrer, D. (1967) Morphological changes of heart muscle caused by successive perfusion with calcium-free and calcium-containing solutions (Calcium paradox). *Cardiovasc. Res.* 1; 201–209.